JOURNAL OF
APPLIED
CRYSTALLOGRAPHY

ISSN 1600-5767

Incorporating the direct derivation method and molecular scattering power method into the Rietveld quantitative phase analysis routine in *TOPAS*

Xiaodong Wang* and Henry Spratt

Central Analytical Research Facility, Queensland University of Technology (QUT), Level 6, P Block, Gardens Point Campus, Brisbane, Queensland, 4001, Australia. *Correspondence e-mail: tony.wang@qut.edu.au

Received 12 December 2024
Accepted 6 May 2025

Edited by R. Guinebretière, Institut de Recherche sur les Céramiques, France

Keywords: direct derivation method; molecular scattering power; Rietveld; quantitative phase analysis; QPA; *TOPAS*.

Supporting information: this article has supporting information at journals.iucr.org/j

The equations of the direct derivation method (DDM) and the unit-cell scattering power method are reviewed in this report. Their relationships and connections to the conventional Rietveld quantitative phase analysis (QPA) are revealed, leading to the development of the C_k-corrected DDM and the molecular scattering power (MSP) method. Both methods can be seamlessly integrated into the conventional Rietveld QPA routine as hybrid QPA, *i.e.* they enable fitting phases of partially or no known crystal structure simultaneously with conventional crystal structure modelling of other known crystalline phases. The accuracies of these hybrid QPA methods are evaluated using a calculated X-ray diffraction pattern for a mixture, the IUCr round robin CPD-1 dataset and synthetic mixtures of disordered source clay minerals (kaolinite KGa-2, chlorite CCa-2) with corundum, using both Launch Mode and Graphical User Interface (GUI) Mode of the *TOPAS* software. Although the accuracies of these hybrid QPA methods are slightly lower than that of conventional Rietveld QPA, their absolute deviations from weighed percentages are scarcely larger than 3 wt%. Compared with the original DDM, the C_k correction enhances QPA accuracy, particularly for mixtures containing phases of large differences in average atomic number. An advantage over the original unit-cell scattering power method is that the proposed MSP method eliminates the need to know the lattice parameters, unit-cell volume or number of molecules in the unit cell.

$$Z_k M_k V_k Scale_k = \frac{a_k S_k}{C_k}$$

$$Z_k M_k V_k Scale_k = \frac{M_k S_k}{\mathrm{mol\_f2}_k}$$

1. Introduction

Conventional Rietveld quantitative phase analysis (QPA) requires that the crystal structures of analytes are known (Hill & Howard, 1987; Bish & Howard, 1988). For QPA involving phases of partially or no known crystal structure, the PONKCS method (Scarlett & Madsen, 2006) can be employed. This method requires a preliminary experimental step to calibrate the *ZMV* factor—the product of unit-cell mass and unit-cell volume—of the PONKCS phase (Wang *et al.*, 2011). Alternatively, calibration can be achieved by refining the atomic occupancies of an uncertain structural model, such as the interlayer exchangeable cations or water content in swelling clay minerals (Wang *et al.*, 2012). These calibration procedures typically involve (1) enriching the unknown phase from the sample to be quantified, (2) preparing a standard mixture—usually in 1:1 weight ratio—of the enriched unknown phase and a well-characterized crystalline standard, and (3) scanning the standard mixture under the same instrument conditions used for all samples containing the unknown phase. Therefore, the application of the PONKCS method is limited to scenarios in which these experimental calibration steps can be performed.

https://doi.org/10.1107/S1600576725004054

The direct derivation method (DDM) (Toraya, 2016) is a relatively new QPA technique primarily developed for phases with unknown crystal structure, offering the distinct advantage of ease of use. DDM calculates the unknown phase's scattering power per unit mass, denoted as a_k^{-1}, from its chemical composition (Toraya, 2017), thereby avoiding the laborious calibration steps required by methods such as PONKCS. As long as the chemical compositions for all the analytes are known, QPA can be performed using DDM via the whole-powder-pattern fitting procedure (Toraya, 2018).

However, the theoretical foundation of DDM assumes that (*a*) the sum of squared structure factors for all reflections within an appropriately wide 2θ range can be approximated by (*b*) the product of unit-cell volume and the sum of squared electron numbers for all atoms in the unit cell—a fixed number for a particular phase (Toraya, 2016). Naturally, the validity of this assumption depends on the appropriateness of the chosen 2θ range. Although the ratios C between (*a*) and (*b*) have been plotted against the upper limit of the 2θ range ($2\theta^{\rm UL}$) for 13 phases and deemed to be 'close' to each other [Fig. 1 of Toraya (2016)], counter-examples have been raised by He & Li (2022), in which the C ratios differ significantly among component phases over any 2θ range, leading to wrong QPA results from DDM that deviate more than 20% from those obtained using the conventional Rietveld QPA method.

Instead, Li *et al.* (2022) proposed a unit-cell scattering power method to estimate the sum of squared structure factors of an analyte by using the sum of squared structure factors of a series of imaginary crystals. Each of these imaginary crystals contains a single constituent atom in the analyte's unit cell positioned at the origin of the same unit cell. An example for corundum is illustrated in Fig. 1.

This approach is based on the principle that the structure factor of a unit cell is the Fourier transform of its electron density. According to Parseval's theorem (Pollard, 1926; Hughes, 1965; Zwillinger, 2014), the sum of squared structure factors equals the integral of squared electron density over the unit cell. If this integral can be approximated by the sum of the squared electron densities of individual atoms in the unit cell, *i.e.* ignoring electrons on interatomic bonds, then the sum of squared structure factors can also be approximated in this manner. This offers an alternative way to evaluate the total scattering power of phases with partially known structures, facilitating phase quantification without requiring knowledge of atomic positions. Unfortunately, the authors did not find suitable software to implement their method and hence devised equations for calculating relative intensity ratios (RIR), a non-refinement-based QPA method (Li & He, 2023).

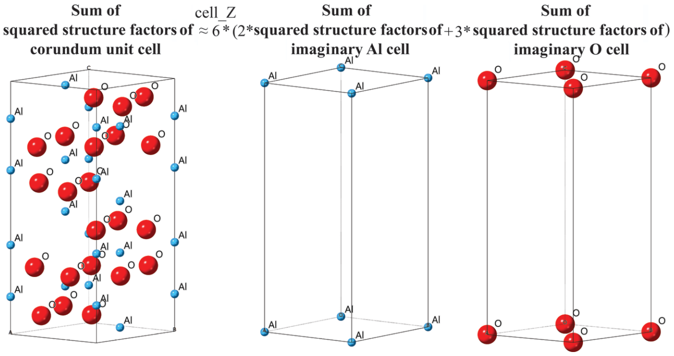

Figure 1
The application of the unit-cell scattering power method (Li *et al.*, 2022) on corundum (α-Al_2O_3). The sum of squared structure factors of a corundum cell can be estimated through the sum of squared structure factors of 12 imaginary Al crystals and 18 imaginary O crystals in the corundum unit cell. 'cell_Z' denotes the number of Al_2O_3 molecules in the corundum unit cell.

The present report reviews the equations used in Rietveld QPA alongside those of DDM and the unit-cell scatting power method, leading to the development of a C_k-corrected DDM and a molecular scattering power (MSP) method, respectively. Both methods are shown to be compatible with the conventional Rietveld QPA routine. Incorporating individual C_k values for different phases improves the QPA accuracy of DDM. The MSP method simplifies analysis by eliminating the need to know the lattice parameters or unit-cell volume of the unknown crystalline phase. Examples are provided using the *TOPAS* v7 software (Coelho, 2018), including INP templates to calculate the C_k ratio for any measured 2θ range, demonstrating Pawley fitting to fit only the unknown phase together with Rietveld refinements for known phases. Equations for C_k-corrected DDM calculations and the MSP method are implemented in the Rietveld QPA routine of both Launch Mode and Graphical User Interface (GUI) Mode in the *TOPAS* v7 software. An INP template is also provided to calculate the MSP value for any chemical formula. Both methods are demonstrated to be equivalent to conventional Rietveld QPA, as theorized by the final equation in Section 2.

2. Theory

2.1. Rietveld QPA

The diffraction intensity of the jth reflection of the kth phase in a multi-phase mixture measured using Bragg–Brentano geometry can be written as (Madsen & Scarlett, 2008)

$$I_{jk} = \left(\frac{I_0\lambda^3}{32\pi r}\frac{e^4}{m_{\rm e}^2c^4}\right)\left[\frac{m_{jk}}{2V_k^2}\left|F_{jk}\right|^2\left(\frac{1+\cos^2 2\theta_{jk}\cos^2 2\theta_{\rm m}}{\sin^2\theta_{jk}\cos\theta_{jk}}\right)\right]\left(\frac{W_k}{\rho_k\mu}\right), \tag{1}$$

where I_0 is the incident beam intensity, λ is the X-ray wavelength, e is the electron charge, $m_{\rm e}$ is the electron mass, r is the goniometer diameter, c is the speed of light, m and F are the multiplicity and structure factor, respectively, V is the unit-cell volume, and θ_j and $\theta_{\rm m}$ are the Bragg angles for the jth sample reflection and for the monochromator, respectively. W_k and ρ_k are the weight fraction and density of phase k, while μ is the mass absorption coefficient of the mixture sample.

We use Q to represent the physical and geometrical constants $[\lambda^3/(32\pi r)][e^4/(2m_{\rm e}^2c^4)]$ and LP_{jk} to represent $(1+\cos^2 2\theta_{jk}\cos^2 2\theta_{\rm m})/(\sin^2\theta_{jk}\cos\theta_{jk})$, the Lorentz and polarization factor. Then substituting $\rho_k = Z_k M_k / V_k$ into equation (1) and summing over all N_k reflections gives

$$S_k = \sum_{j=1}^{N_k} \frac{I_{jk}}{\mathrm{LP}_{jk}} = \frac{I_0 Q}{\mu} \frac{W_k}{Z_k M_k V_k} \sum_{j=1}^{N_k} m_{jk} \left| F_{jk} \right|^2, \tag{2}$$

where M_k is the molecular weight and Z_k is the number of molecules in unit cell. For simplicity, the LP-factor-corrected diffraction intensity in equation (2) is denoted as S_k. Rearranging equation (2) provides the weight fraction of phase k:

$$W_k = \frac{\mu}{I_0 Q} Z_k M_k V_k \frac{S_k}{\sum_{j=1}^{N_k} m_{jk} \left| F_{jk} \right|^2}. \tag{3}$$

In Rietveld QPA, the last term of equation (3)—the ratio between the sum of LP-factor-corrected intensities S_k and the sum of structure factors—is refined as the Rietveld scale factor:

$$\mathrm{Scale}_k = \frac{S_k}{\sum_{j=1}^{N_k} m_{jk} \left| F_{jk} \right|^2}. \tag{4}$$

Among all K component crystalline phases in the mixture, the relative weight fraction of phase k can be derived as

$$W_k = \frac{Z_k M_k V_k \,\mathrm{Scale}_k}{\sum_{k'=1}^{K} Z_{k'} M_{k'} V_{k'} \,\mathrm{Scale}_{k'}}. \tag{5}$$

Equation (5) is widely used in many Rietveld software platforms that are currently publicly available for QPA and is hereafter referred to as 'Rietveld QPA'.

2.2. C_k-corrected direct derivation method

Toraya (2016) pointed out [equation (8) therein] that the scattering power of phase k, calculated from its crystal structure in Rietveld QPA as the sum of squared structure factors [*i.e.* the denominator of equation (4)], can be approximated using a formula involving the sum of squared electron numbers of each atom, which can be calculated directly from the chemical formula of phase k:

$$\sum_{j=1}^{N_k} m_{jk} \left| F_{jk} \right|^2 = C_k V_k Z_k \sum_{i=1}^{A_k} n_i^2. \tag{6}$$

In the right-hand term of equation (6), n_i is the electron number for the ith atom out of a total of A_k atoms in the chemical formula (hereafter 'molecule'), while C_k is the ratio between these two forms of X-ray scattering power for phase k. With the above replacement, equation (3) can be written as

$$W_k = \frac{\mu}{I_0 Q} M_k \frac{S_k}{C_k \sum_{i=1}^{A_k} n_i^2}. \tag{7}$$

Toraya (2017) further grouped the parameters originating from the nature of the phase k as a_k,

$$a_k = \frac{M_k}{\sum_{i=1}^{A_k} n_i^2}, \tag{8}$$

where the physical meaning of a_k^{-1} is the scattering intensity per unit mass of phase k. Therefore, the equivalent relative weight fraction of phase k in DDM follows equation (9),

$$W_k = \frac{a_k S_k / C_k}{\sum_{k'=1}^{K} a_{k'} S_{k'} / C_{k'}}, \tag{9}$$

except that C_k was assumed to be the same for all phases and hence got cancelled in the original DDM (Toraya, 2016). Comparing equation (9) and equation (5), it is easy to find the relationship between DDM and the conventional Rietveld QPA:

$$Z_k M_k V_k \,\mathrm{Scale}_k = \frac{a_k S_k}{C_k}. \tag{10}$$

Equation (10) allows incorporation of a C_k-corrected DDM calculation for phase k into the conventional Rietveld QPA routine, avoiding any experimental calibration step for the *ZMV* factor in the PONKCS method if the value of C_k is known.

For poorly crystalline phases—such as those exhibiting severe structural disorder—conventional Rietveld refinement may not adequately fit the area under the diffraction peaks, from which QPA results are derived. In general, Pawley or Le Bail fitting (*TOPAS* `hkl_Is` model) and the peaks phase fitting (*TOPAS* `xo_Is` model) provide better fits to the peak areas and shapes of the whole powder pattern than the Rietveld method (*TOPAS* `str` model), because of their individual control of peak intensities, profiles and positions. With a C_k value calculated from a sufficiently similar, disorder-free crystal structure of the same or similar phase (available from crystal structure databases), equation (9) enables quantification of disordered or poorly crystalline phases using `hkl_Is` models (Pawley or Le Bail fitting) or `xo_Is` models (whole-powder-pattern fitting), without the need to explicitly model disorder-induced peak profile changes.

2.3. Molecular scattering power method

Li *et al.* (2022) revisited equation (3) and proposed the unit-cell scattering power method. It approximates the sum of squared structure factors for the unit cell of phase k [the denominator of equation (4)] using the sum of squared structure factors from a series of imaginary crystals of the same unit cell, each with only a single constituent atom of phase k placed at their origins (as has been illustrated in Fig. 1):

$$\sum_{j=1}^{N_k} m_{jk} \left| F_{jk} \right|^2 = \sum_{i=1}^{N} \sum_{h'} f_{ih'}^2. \tag{11}$$

In the right-hand term of equation (11), $f_{ih'}^2$ stands for the squared structure factor of the h' reflection from imaginary crystals consisting of only the ith atom—out of a total of $N = Z_k A_k$ constituent atoms in the phase k unit cell—sitting at the origin of the unit cell of phase k. Although this unit-cell scattering power approach does not require atomic position information, it still relies on the known lattice parameters and the molecular motif of the target phase k.

However, if one studies the equations provided by Li *et al.* (2022), the requirement of 'known lattice parameters' is not necessary. Following the idea of Li *et al.* (2022), since the structure factor F_{hkl} is the Fourier transform of the electron density distribution $\rho(\mathbf{r})$ in the unit cell, according to Parseval's theorem (Pollard, 1926; Hughes, 1965; Zwillinger, 2014), the sum of squared structure factors $\sum |F_{hkl}|^2$ equals the integral of the squared electron density distribution $\rho(\mathbf{r})$ over the unit cell:[1]

$$\sum_{hkl} |F_{hkl}|^2 = \sum_{j=1}^{N_k} m_{jk} |F_{jk}|^2 = V_k \int_{V_k} \rho^2(\mathbf{r})\ \mathrm{d}v \qquad (12)$$

If the electron density distribution of the unit cell can be approximated by the sum of the electron density distributions of isolated atoms, *i.e.* ignoring the electron density charges on interatomic bonds, then the squared electron density distribution of the unit cell $\rho^2(\mathbf{r})$ can be approximated by the sum of squared electron density $\rho_i^2(\mathbf{r}_i)$ of each atom for all $Z_k A_k$ atoms in the unit cell, or in a mathematical expression

$$\int_{V_k} \rho^2(\mathbf{r})\ \mathrm{d}v = Z_k \sum_{i=1}^{A_k} \int_{V_k} \rho_i^2(\mathbf{r}_i)\ \mathrm{d}v. \qquad (13)$$

Considering the last integral in equation (13), the integration volume V_k (unit-cell volume of phase k) is commonly much larger than the atomic volumes, outside of which $\rho_i(\mathbf{r}_i)$ reaches zero. The integration result, therefore, does not depend on V_k the region of integration, *i.e.* the following relation holds for the same atom:

$$\int_{V_k} \rho_i^2(\mathbf{r}_i)\ \mathrm{d}v = \int_{V_\mathrm{d}} \rho_i^2(\mathbf{r}_i)\ \mathrm{d}v, \qquad (14)$$

where V_d is any arbitrary dummy volume providing it is much larger than the atomic volumes. If we create A_k imaginary crystals in arbitrary dummy unit cells (*e.g.* cubic cells of lattice parameter a = 10 Å) and place each constituent atom of the phase k molecule on their origins (space group $P1$, $x = y = z = 0$), the following relation holds for these imaginary crystals [*cf.* equations (12) and (13)]:

$$\frac{1}{V_\mathrm{d}} \sum_{j=1}^{N_\mathrm{d}} m_{j\mathrm{d}} |f_{j\mathrm{d}}|^2 = Z_\mathrm{d} \sum_{i=1}^{A_\mathrm{d}} \int_{V_\mathrm{d}} \rho_i^2(\mathbf{r}_i)\ \mathrm{d}v = \int_{V_\mathrm{d}} \rho_i^2(\mathbf{r}_i)\ \mathrm{d}v, \qquad (15)$$

where $m_{j\mathrm{d}}$ and $f_{j\mathrm{d}}$ are the multiplicity and structure factor, respectively, of the jth reflections (j = 1 to N_d) from the imaginary dummy crystals. Since there is only one atom in these dummy cells, $Z_\mathrm{d} = A_\mathrm{d} = 1$. Bringing equations (12)–(15) together we have

$$\mathrm{mol\_f2}_k = \frac{\sum_{j=1}^{N_k} m_{jk} |F_{jk}|^2}{V_k Z_k} = \sum_{i=1}^{A_k} \left(\frac{\sum_{j=1}^{N_\mathrm{d}} m_{j\mathrm{d}} |f_{j\mathrm{d}}|^2}{V_\mathrm{d}} \right). \qquad (16)$$

This means that the molecular scattering power of phase k [the middle part of equation (16), hereafter denoted as '$\mathrm{mol\_f2}_k$'], which is the unit-cell scattering power divided by the cell volume V_k and the number of molecules in the unit cell Z_k, can be approximated by the sum of squared structure factors of the A_k arbitrary dummy cells divided by the dummy cell volume V_d, as schematized in Fig. 2. Since the dummy cells contain only a single constituent atom each at their origins, the part in brackets of equation (16) is, in fact, the atomic scattering power of each constituent atom (sum of the squared product of the atomic form factor and its atomic displacement parameter).

Substituting equation (16) back into equation (3), we have

$$W_k = \frac{\mu}{I_0 Q} M_k \frac{S_k}{\mathrm{mol\_f2}_k}. \qquad (17)$$

The weight percentage of phase k in a K-crystalline-phase mixture can, therefore, be expressed as

$$W_k = \frac{M_k S_k / \mathrm{mol\_f2}_k}{\sum_{k'=1}^{K} M_{k'} S_{k'} / \mathrm{mol\_f2}_{k'}}. \qquad (18)$$

With Z_k and V_k cancelled out, the expression of equation (18) is much simpler than the form proposed by Li *et al.* (2022) [equation (18) therein], meaning that it is not necessary to know the number of molecules in the unit cell Z_k, the lattice parameters or the unit-cell volume V_k when applying the MSP method to perform QPA for an unknown crystalline phase. Comparing this MSP method [equation (18)] with the conventional Rietveld QPA [equation (5)] reveals their relationship:

$$Z_k M_k V_k\ \mathrm{Scale}_k = \frac{M_k S_k}{\mathrm{mol\_f2}_k}. \qquad (19)$$

Equation (19) in fact conveys a similar concept to the intensity–composition equation of DDM (Toraya, 2021): the weight of a phase equals its diffraction intensity divided by its scattering power per unit mass. By comparing equation (19) with equation (10), we can derive the relationship between the conventional Rietveld QPA, the C_k-corrected DDM and the MSP method:

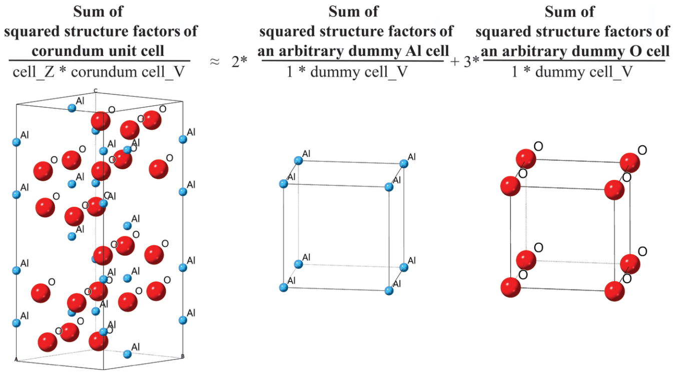

Figure 2
Example of the MSP method applied on corundum (α-Al_2O_3). The sum of squared structure factors of an Al_2O_3 molecule (unit-cell scattering power divided by the cell volume 'cell_V' and the number of molecules in the unit cell 'cell_Z') can be estimated by the sum of squared structure factors of two imaginary Al crystals and three imaginary O crystals in any arbitrary dummy cell, divided by the dummy cell volume (atomic scattering power).

---

[1] Equivalent forms of equation (12) have also been reported elsewhere (Hettich, 1935; Sayre, 1951; Kartha, 1953).

$$Z_k M_k V_k \,\mathrm{Scale}_k = \frac{a_k S_k}{C_k} = \frac{M_k S_k}{C_k \sum_{i=1}^{A_k} n_i^2} = \frac{M_k S_k}{\mathrm{mol\_f2}_k}. \qquad (20)$$

It is easy to see from equation (20) that the molecular scattering power mol_f2$_k$ is equivalent to the 'C_k-corrected sum of squared electron numbers' in the C_k-corrected DDM approach. As pointed out in the explanation of equation (16), mol_f2$_k$ is essentially a sum of atomic scattering powers (sum of the squared product of atomic form factor and atomic displacement parameter), which change with radiation wavelength for a fixed 2θ range, while the sum of n_i^2 value used in DDM is merely a constant. Therefore, it is necessary to apply the proposed C_k correction for DDM in order to reduce the discrepancies between the sum of squared electron numbers and mol_f2$_k$. Equation (19) allows the incorporation of the MSP method for phase k of unknown crystal structure into the conventional Rietveld QPA routine.

2.4. Calculation of molecular scattering power mol_f2

The molecular scattering power mol_f2 of any chemical formula can be conveniently calculated through the right-hand term of equation (16) in the *TOPAS* software. Using the INP template provided in Section S1 of the supporting information, it took a laptop (Intel i7-1185 G7 @ 3 GHz 1.8 GHz, 16 GB RAM) less than 1 s to calculate the scattering power of the Al_2O_3 molecule and save it into a `mol_f2_corundum.inc` file for the subsequent QPA INP to call. The MSP mol_f2 values for several crystalline phases are plotted against the used dummy cell volumes V_d in Fig. 3.

It is easy to see from Fig. 3 that, except for the smallest dummy cell of 1 Å^3 (not larger than the Al or O atomic volumes), the MSP mol_f2 values are almost constant no matter what sizes of dummy cell were used to calculate them. This validates equation (14). Some fluctuations of zincite, corundum and fluorite are believed to be due to the 'termination effect' in calculating the sum of structure factors (Toraya, 2022). The MSP mol_f2 values are stabilized when a large dummy cell (*e.g.* a cubic cell of lattice parameter a = 10 Å) is used to generate many *hkl* reflections.

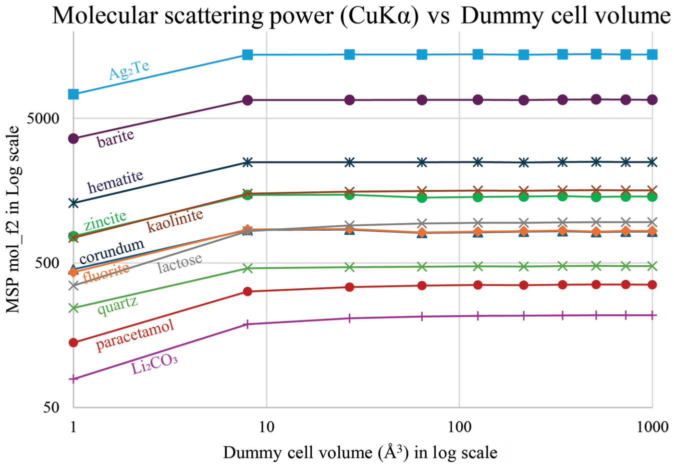

Figure 3
The molecular scattering powers of several crystalline phases under Cu *Kα* radiation plotted against the volumes of dummy cubic cells used to calculate them.

3. Implementations in the *TOPAS* software

It has been proposed that the *TOPAS* keyword `numerical_area` could be used to implement DDM. However, `numerical_area` was not designed to remove the LP factor (see Appendix *A*). Therefore, it is not equivalent to the S_k parameter in DDM calculation (Toraya, 2017). The following analysis steps are proposed to implement the C_k-corrected DDM calculation and the MSP method in *TOPAS* v7 using the `I` parameters in Pawley phase `hkl_Is` and peaks phase `xo_Is` fitting.

3.1. Analysis steps for C_k-corrected DDM

(*a*) A *TOPAS* template `cal_C.inp` exporting the C_k value for a crystalline phase is described in Section S2 of the supporting information. Using this template, readers can calculate the C_k value of any analyte for the scanned wavelength and 2θ range. The result is saved into a `.inc` file for the subsequent QPA INP to call.

(*b*) Apply Pawley or Le Bail fitting using the `hkl_Is` model to extract the peak area of the crystalline phase of partially known structure, together with Rietveld fitting for other phases of known crystal structure. The sum of all the extracted and fixed `I` values in the `hkl_Is` phase is assigned to a parameter S_k. The `Scale` keyword is not used in `hkl_Is` phases and hence equals 1.

(*c*) Calculate the molecular weight M_k and the total squared electron numbers for each atom in the molecule $\sum_{i=1}^{A_k} n_i^2$. With the C_k value determined in step (*a*), a `DDM_aS_on_C` value for this phase is calculated as $(M_k S_k / \sum_{i=1}^{A_k} n_i^2)/C_k$, which is equivalent to the $Z_k M_k V_k$ Scale$_k$ factor in Rietveld QPA. Use the value of `DDM_aS_on_C / cell_volume` as the `cell_mass` ($Z_k M_k$) in the `hkl_Is` model.

(*d*) Execute the same `.inp` file again; the Rietveld QPA routine in *TOPAS* will report the weight percentages of all the component phases, including the DDM-modelled unknown phase, according to equation (5).

3.2. Analysis steps for molecular scattering power method

(*a*) As shown in Section 2.4, use the *TOPAS* INP template described in Section S1 of the supporting information to calculate the MSP mol_f2 value for the chemical formula (molecule) of any phase of partially or no known crystal structure, providing its chemical formula is known.

(*b*) Same as Step (*b*) in Section 3.1, if the lattice parameters are known for the target phase. Otherwise use the `xo_Is` model to fit the peak area of the phase of no known structure, together with Rietveld fits for other phases of known crystal structure. The sum of all the extracted and fixed `I` values in the `xo_Is` model is assigned to a parameter S_k. The `Scale` keyword is not used in the `xo_Is` phase and hence equals 1.

Table 1
QPA results of the XRD pattern calculated from a 1:1 weight ratio of Ag_2Te and Li_2CO_3 using different combinations of QPA methods: R – Rietveld QPA; D – C_k-corrected DDM; f – MSP method.

	Choices of QPA methods used for Ag_2Te (hessite) and Li_2CO_3 (zabuyelite), respectively						
	R R	D R	R D	D D	R f	f R	f f
Ag_2Te wt%	49.986 (7)	49.867 (5)	49.320 (1)	49.187 (1)	52.144 (1)	49.420 (5)	51.556 (1)

(*c*) Calculate the molecular weight M_k. With the MSP mol_f2 value determined in step (*a*), the value of $M_k S_k/\text{mol\_f2}_k$ can be used as the `cell_mass` of the `xo_Is` model, in which its cell volume is set to 1, according to equation (19). In the case of using the `hkl_Is` model, V_k is calculated from the known lattice parameters. Therefore, use the value of $(M_k S_k/\text{mol\_f2}_k)$/cell_volume as the `cell_mass` of the `hkl_Is` model.

(*d*) Same as Step (*d*) in Section 3.1.

4. Examples

4.1. Test on the calculated XRD pattern for a 1:1 weight mixture of Ag_2Te and Li_2CO_3

This extreme counter-example was used in He & Li's (2022) comment on DDM, which highlighted the fact that *C* values are phase dependent. Ignoring their differences may lead to wrong QPA results. The current analysis steps propose to include C_k into the DDM calculation to make it compatible with the conventional Rietveld QPA routine.

The *TOPAS* file `Ag2Te_Li2CO3_mixture.inp` and the calculated XRD pattern for a 1:1 weight mixture of Ag_2Te and Li_2CO_3 are available in the supporting information. The calculated C_k value for hessite, Ag_2Te, is 1.91, while the C_k value for zabuyelite, Li_2CO_3, is 0.79. The INP file contains `str` models and `hkl_Is` models for both phases. In total, four combinations of model choices are considered, and the QPA results reported in the corresponding OUT file are summarized in the first four columns of Table 1. Since the weight percentage sum of Ag_2Te and Li_2CO_3 phases is 100%, only Ag_2Te wt% results are shown in Table 1. The full-pattern fits using the C_k-corrected DDM for both phases are shown in Fig. 4.

Table 1 indicates that, by bringing back the C_k correction into equation (9), accurate or reasonable QPA results are achieved even for this extreme counter-example, in contrast to the wrong QPA results (more than 20 wt% discrepancy) obtained through the original DDM as pointed out by He & Li (2022). This example serves the purpose of validating the effectiveness of equation (9), *i.e.* the rectification effect of C_k on top of the original DDM.

Analogously, the MSP method proposed in this paper is tested on this example, and the QPA results are reported in the last three columns of Table 1. The MPS method is also able to deliver QPA results of reasonable accuracy for this example, validating the effectiveness of equation (18). The full-pattern fitting modelled by the same `hkl_Is` phases is identical to that in Fig. 4 and is hence omitted. The implemented MSP QPA equations are also stored in the same *TOPAS* INP file in the supporting information. A global level selection is devised to allow user toggling between the C_k-corrected DDM and the MSP mol_f2 method.

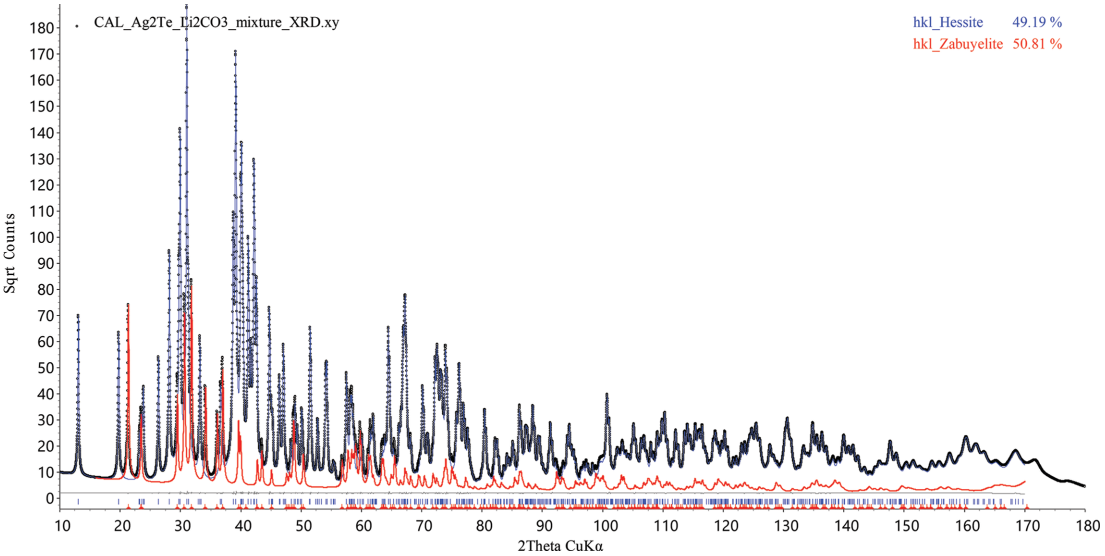

Figure 4
Full pattern refinement of the calculated XRD pattern of 1:1 weight ratio of hessite (Ag_2Te) and zabuyelite (Li_2CO_3), using the C_k-corrected DDM for both phases (D D in Table 1). The calculated data are shown as black dots. The contribution of hessite is shown as the blue curve, while that of zabuyelite is highlighted as the red curve.

Table 2
The discrepancies of QPA results from the weighed weight percentages of the three-phase mixtures of the CPD-1 series samples using the various proposed QPA methods.

R – Rietveld QPA; D – C_k-corrected DDM; f – MSP method using Pawley fitting (`hkl_Is`); x – MSP method using peaks phases (`xo_Is`). Their orders represent the corresponding model used for corundum, fluorite and zincite, respectively. The column 'D D D no C_k' stands for the original DDM calculation without C_k correction. The numbers in brackets are the refinement errors aligned for the last decimal place.

			Rietveld	C_k-corrected DDM							Original DDM
Sample ID	Weighed wt%		R R R	R R D	R D R	R D D	D R R	D R D	D D R	D D D	D D D no C_k
CPD-1a	Corundum	1.15	0.09 (7)	0.11 (7)	0.10 (7)	0.12 (7)	0.57 (18)	0.57 (18)	0.59 (18)	0.59 (18)	0.70 (19)
	Fluorite	94.81	0.14 (8)	0.18 (10)	0.08 (8)	0.12 (10)	−0.34 (18)	−0.27 (18)	−0.41 (18)	−0.33 (19)	−0.7 (2)
	Zincite	4.04	−0.23 (4)	−0.29 (7)	−0.18 (4)	−0.24 (7)	−0.23 (4)	−0.30 (7)	−0.18 (4)	−0.26 (7)	−0.01 (8)
CPD-1b	Corundum	94.31	0.12 (4)	−0.11 (6)	0.32 (6)	0.11 (8)	0.14 (4)	0.05 (6)	0.35 (6)	0.18 (8)	0.41 (7)
	Fluorite	4.33	−0.14 (4)	−0.12 (4)	−0.35 (6)	−0.33 (6)	−0.16 (4)	−0.16 (4)	−0.38 (6)	−0.39 (6)	−0.62 (5)
	Zincite	1.36	0.02 (2)	0.23 (6)	0.03 (2)	0.23 (6)	0.02 (2)	0.20 (5)	0.03 (2)	0.21 (5)	0.22 (6)
CPD-1c	Corundum	5.04	0.75 (11)	0.67 (11)	0.80 (11)	0.64 (11)	2.5 (4)	2.5 (4)	2.4 (4)	2.4 (4)	2.4 (4)
	Fluorite	1.36	0.02 (4)	0.02 (4)	0.42 (10)	0.42 (10)	0.02 (4)	0.03 (4)	0.39 (10)	0.4 (1)	0.28 (9)
	Zincite	93.59	−0.76 (11)	−0.68 (11)	−1.21 (14)	−1.06 (14)	−2.5 (4)	−2.5 (4)	−2.8 (4)	−2.8 (4)	−2.7 (4)
CPD-1d	Corundum	13.53	1.03 (11)	1.09 (11)	1.17 (11)	1.23 (11)	0.9 (2)	1.0 (2)	1.1 (2)	1.1 (2)	1.6 (2)
	Fluorite	53.58	−0.59 (11)	−0.47 (11)	−1.02 (12)	−0.90 (12)	−0.54 (15)	−0.39 (15)	−0.98 (15)	−0.84 (16)	−2.51 (16)
	Zincite	32.89	−0.44 (9)	−0.62 (10)	−0.15 (9)	−0.32 (11)	−0.40 (11)	−0.59 (12)	−0.10 (11)	−0.28 (12)	0.92 (13)
CPD-1e	Corundum	55.12	1.38 (9)	1.41 (10)	1.66 (10)	1.66 (11)	1.52 (11)	1.55 (12)	1.76 (12)	1.79 (13)	2.88 (12)
	Fluorite	29.62	−0.73 (8)	−0.74 (8)	−1.05 (10)	−1.04 (10)	−0.84 (9)	−0.82 (9)	−1.14 (10)	−1.13 (11)	−2.49 (10)
	Zincite	15.25	−0.64 (5)	−0.66 (7)	−0.60 (5)	−0.61 (7)	−0.67 (6)	−0.72 (8)	−0.61 (6)	−0.66 (8)	−0.38 (7)
CPD-1f	Corundum	27.06	1.24 (12)	1.34 (12)	1.41 (12)	1.51 (12)	1.21 (19)	1.32 (19)	1.37 (19)	1.48 (19)	1.74 (19)
	Fluorite	17.72	−0.14 (7)	−0.05 (7)	−0.58 (10)	−0.51 (10)	−0.13 (8)	−0.04 (8)	−0.57 (10)	−0.50 (10)	−1.43 (10)
	Zincite	55.22	−1.10 (10)	−1.29 (11)	−0.83 (11)	−1.00 (12)	−1.08 (15)	−1.28 (16)	−0.80 (16)	−0.98 (16)	−0.30 (16)
CPD-1g	Corundum	31.37	1.26 (11)	1.29 (11)	1.43 (12)	1.46 (12)	1.75 (17)	1.81 (17)	1.92 (17)	1.98 (17)	2.64 (18)
	Fluorite	34.42	−0.60 (9)	−0.51 (9)	−0.91 (11)	−0.84 (11)	−0.83 (17)	−0.76 (11)	−1.16 (12)	−1.10 (13)	−2.55 (12)
	Zincite	34.21	−0.67 (8)	−0.78 (9)	−0.52 (9)	−0.62 (10)	−0.62 (11)	−1.05 (11)	−0.76 (11)	−0.88 (12)	−0.09 (12)
CPD-1h	Corundum	35.12	1.01 (11)	1.09 (11)	1.27 (12)	1.36 (12)	1.08 (16)	1.18 (16)	1.33 (16)	1.45 (16)	2.20 (17)
	Fluorite	34.69	−0.33 (9)	−0.19 (9)	−0.79 (11)	−0.67 (11)	−0.36 (11)	−0.24 (11)	−0.83 (12)	−0.72 (12)	−2.19 (12)
	Zincite	30.19	−0.69 (8)	−0.89 (9)	−0.48 (8)	−0.69 (9)	−0.71 (9)	−0.94 (10)	−0.50 (10)	−0.73 (11)	−0.01 (11)

			MSP using `hkl_Is`							MSP using `xo_Is`		
Sample ID	Weighed wt%		R R f	R f R	R f f	f R R	f R f	f f R	f f f	R R x	R x R	x R R
CPD-1a	Corundum	1.15	0.11 (7)	0.18 (7)	0.21 (8)	0.49 (17)	0.49 (17)	0.61 (18)	0.62 (18)	0.07 (8)	0.15 (8)	0.81 (19)
	Fluorite	94.81	0.36 (9)	−0.25 (8)	−0.01 (10)	−0.26 (17)	−0.00 (17)	−0.68 (18)	−0.41 (19)	0.39 (10)	−0.26 (9)	−0.61 (18)
	Zincite	4.04	−0.47 (7)	0.07 (4)	−0.20 (7)	−0.23 (4)	−0.49 (7)	0.07 (4)	−0.21 (7)	−0.46 (7)	0.11 (5)	−0.21 (4)
CPD-1b	Corundum	94.31	−0.03 (6)	0.56 (6)	0.42 (7)	−0.13 (4)	−0.25 (6)	0.33 (6)	0.24 (8)	−0.02 (6)	0.56 (6)	−0.19 (5)
	Fluorite	4.33	−0.12 (4)	−0.59 (5)	−0.58 (5)	0.04 (4)	0.05 (4)	−0.44 (5)	−0.44 (6)	−0.12 (4)	−0.59 (5)	0.09 (4)
	Zincite	1.36	0.15 (5)	0.03 (2)	0.15 (5)	0.09 (2)	0.20 (5)	0.10 (2)	0.21 (5)	0.14 (5)	0.03 (2)	0.09 (2)
CPD-1c	Corundum	5.04	0.95 (11)	0.80 (11)	0.93 (11)	2.1 (4)	2.5 (4)	2.1 (4)	2.5 (4)	1.03 (11)	0.81 (11)	1.7 (4)
	Fluorite	1.36	0.09 (4)	0.31 (10)	0.40 (10)	0.02 (4)	0.10 (4)	0.29 (9)	0.37 (10)	0.10 (4)	0.31 (10)	0.03 (4)
	Zincite	93.59	−1.03 (12)	−1.10 (14)	−1.32 (14)	−2.1 (4)	−2.6 (4)	−2.4 (4)	−2.8 (4)	−1.12 (12)	−1.11 (14)	−1.7 (3)
CPD-1d	Corundum	13.53	1.33 (11)	1.68 (12)	2.00 (12)	0.32 (19)	0.6 (2)	0.9 (2)	1.2 (2)	1.33 (11)	1.70 (12)	0.2 (2)
	Fluorite	53.58	0.43 (11)	−2.67 (12)	−1.65 (12)	−0.16 (14)	0.90 (15)	−2.24 (15)	−1.18 (16)	0.44 (11)	−2.72 (12)	−0.10 (15)
	Zincite	32.89	−1.76 (10)	0.99 (9)	−0.35 (11)	−0.16 (10)	−1.50 (11)	1.30 (11)	−0.06 (12)	−1.77 (10)	1.02 (9)	−0.14 (11)
CPD-1e	Corundum	55.12	1.84 (10)	2.71 (10)	3.16 (11)	0.26 (11)	0.72 (12)	1.56 (12)	2.04 (13)	1.85 (10)	2.78 (10)	0.49 (13)
	Fluorite	29.62	−0.52 (8)	−2.38 (9)	−2.15 (10)	−0.01 (9)	0.25 (9)	−1.66 (10)	−1.42 (11)	−0.49 (8)	−2.46 (9)	−0.11 (10)
	Zincite	15.25	−1.31 (7)	−0.32 (5)	−1.00 (7)	−0.25 (6)	−0.96 (7)	0.11 (6)	−0.62 (8)	−1.35 (7)	−0.31 (5)	−0.36 (6)
CPD-1f	Corundum	27.06	2.15 (12)	1.72 (12)	2.66 (12)	0.19 (18)	1.09 (19)	0.65 (19)	1.58 (19)	2.15 (12)	1.72 (12)	2.29 (4)
	Fluorite	17.72	0.45 (8)	−1.49 (9)	−0.95 (9)	0.12 (8)	0.73 (8)	−1.25 (10)	0.70 (10)	0.45 (8)	−1.49 (9)	−0.38 (7)
	Zincite	55.22	−2.60 (11)	−0.23 (11)	−1.71 (12)	−0.31 (15)	−1.82 (16)	0.60 (16)	−0.88 (16)	−2.60 (11)	−0.23 (11)	−1.91 (6)
CPD-1g	Corundum	31.37	1.86 (12)	2.15 (12)	2.78 (12)	0.63 (17)	1.25 (17)	1.50 (17)	2.16 (17)	1.87 (12)	2.12 (12)	0.94 (18)
	Fluorite	34.42	−0.08 (10)	−2.36 (10)	−1.71 (11)	−0.27 (11)	0.41 (11)	−2.05 (12)	−1.41 (13)	0.08 (10)	−2.36 (10)	−0.35 (12)
	Zincite	34.21	−1.94 (9)	0.22 (9)	−1.07 (10)	−0.36 (10)	−1.66 (11)	0.55 (11)	−0.75 (12)	−1.94 (9)	0.24 (9)	−0.49 (11)
CPD-1h	Corundum	35.12	1.64 (11)	2.08 (12)	2.76 (12)	−0.10 (16)	0.55 (16)	0.94 (16)	1.65 (16)	1.68 (12)	2.15 (12)	0.37 (18)
	Fluorite	34.69	0.33 (9)	−2.25 (10)	−1.62 (11)	0.27 (11)	0.94 (11)	−1.68 (12)	−1.03 (12)	0.34 (10)	−2.34 (11)	0.04 (12)
	Zincite	30.19	−1.97 (9)	0.18 (8)	−1.13 (9)	−0.17 (9)	−1.49 (10)	0.73 (10)	−0.61 (11)	−2.01 (9)	0.20 (9)	−0.41 (10)

4.2. Test on the IUCr round robin CPD-1 series dataset

Eight publicly available XRD patterns (from `CPD-1A.raw` to `CPD-1H.raw`, see *Data availability* section) measured for three-phase mixtures (corundum, fluorite and zincite) of known weighed mass percentages (Madsen *et al.*, 2001) were used to test the accuracy of the analysis steps proposed in Section 3. The file header of the *TOPAS* INP (`Cpd-1a.inp` to `Cpd-1h.inp` in the supporting information) allows readers to toggle between the C_k-corrected DDM and the MSP method. The S_k values were set using *TOPAS* keyword `prm_with_error` to propagate intensity errors into those of the QPA results. Each phase has both structure `str` and `hkl_Is` models set up for selection. The calculated C_k values for corundum, fluorite and zincite are 1.48, 1.39 and 1.49, respectively. The calculated MSP $\mathrm{mol\_f2}_k$ values for them are 825.609, 832.917 and 1509.435, respectively. The same thermal vibration parameters `beq` used in the Rietveld QPA were used in the calculation of these values. The macros `AW` and `AN` return atomic weight and atomic number, respectively (available in supporting information Section S3).

The QPA results using all eight combinations of Rietveld QPA and the C_k-corrected DDM for these three-phase mixtures are summarized in the 'C_k-corrected DDM' columns of Table 2, together with the weighed percentages and the QPA results from the original DDM method without C_k corrections. These QPA results are also plotted on a ternary phase diagram (Fig. S1) to visualize their accuracies and precisions.

Table 2 and Fig. S1 show that the QPA results from the proposed C_k-corrected DDM hybrid with Rietveld QPA are generally more accurate than the results from the original DDM without C_k correction. This set of QPA results suggest that C_k correction for each phase improves DDM accuracy. However, if individual C_k values (requiring crystal structure) are not available, omitting this correction does not change the QPA results too much (<3 wt%) for this dataset, in which the average atomic numbers between phases are not as far apart as they are in the first example in Section 4.1.

Analogously, the QPA results using all eight combinations of Rietveld QPA and the MSP method using Pawley fitting (`hkl_Is`) for these three-phase mixtures are summarized in the 'MSP using `hkl_Is`' columns of Table 2. These QPA results are also plotted on a ternary phase diagram (Fig. S2) to visualize their accuracies and precisions. It can be seen from Table 2 and Fig. S2 that, compared with C_k-corrected DDM, although slightly worse QPA accuracies and precisions are observed, their deviations from the weighed weight percentages are scarcely higher than 3 wt%. The benefit of this MSP method is that it totally eliminates the requirement of knowing the crystal structure (atomic positions).

4.3. Applying the MSP method for phases of unknown lattice parameters

The procedure of Section 3.2 is also tested on the CPD-1 series dataset, assuming the lattice parameters of the target phases are also not known. The *TOPAS* INP files (`Cpd-1a_xo_Is.inp` to `Cpd-1h_xo_Is.inp`) in the supporting information include equation (19) derived for the target phases, without using any lattice parameter, as shown in Fig. 5(*a*). The same operation in *TOPAS* GUI Mode is shown in Fig. 5(*b*). The peaks phase model `xo_Is` [also called the Type A fitting function by Toraya (2018, 2019)] is used in these examples.

The peak positions in the `xo_Is` model are not constrained by lattice parameters as they are in Pawley fitting (`hkl_Is` model). Owing to the inevitable peak overlapping of multiphase powder patterns, simultaneous fitting of two or more unknown phases using peaks phases (`xo_Is` model) will not partition the intensity correctly. Therefore, only four combinations of Rietveld QPA and the MSP method using the `xo_Is` model for the three-phase mixtures in the CPD-1 series were tested, and their results are summarized in the 'MSP using `xo_Is`' columns in Table 2. These QPA results are also plotted on a ternary phase diagram in Fig. S3. From Table 2 and Fig. S3, compared with the MSP method using Pawley fitting (`hkl_Is`), similar levels of QPA discrepancy from weighed percentages (<3 wt%) are observed.

Figs. S1–S3 show that all methods, including the conventional Rietveld method, overestimate corundum. This is

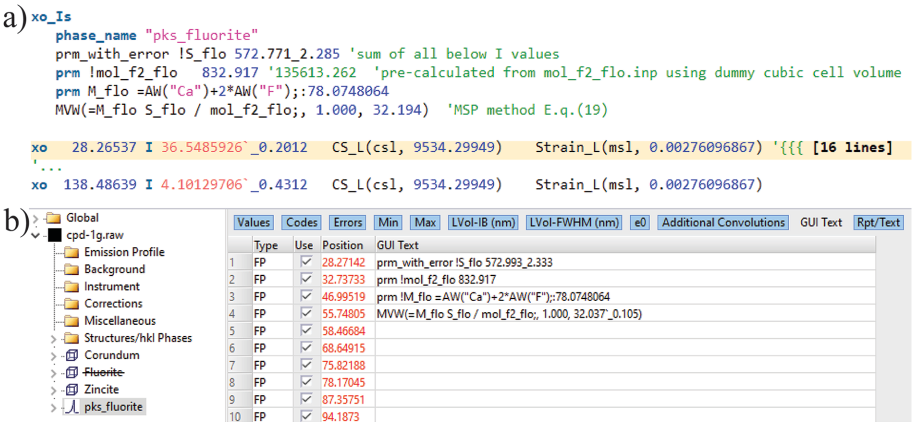

```
xo_Is
   phase_name "pks_fluorite"
   prm_with_error !S_flo 572.771_2.285 'sum of all below I values
   prm !mol_f2_flo   832.917 '135613.262  'pre-calculated from mol_f2_flo.inp using dummy cubic cell volume
   prm M_flo =AW("Ca")+2*AW("F");:78.0748064
   MVW(=M_flo S_flo / mol_f2_flo;, 1.000, 32.194)  'MSP method E.q.(19)

xo   28.26537 I 36.5485926`_0.2012   CS_L(csl, 9534.29949)    Strain_L(msl, 0.00276096867) '{{{ [16 lines]
'...
xo  138.48639 I 4.10129706`_0.4312   CS_L(csl, 9534.29949)    Strain_L(msl, 0.00276096867)
```

	Type	Use	Position	GUI Text
1	FP	☑	28.27142	prm_with_error !S_flo 572.993_2.333
2	FP	☑	32.73733	prm !mol_f2_flo 832.917
3	FP	☑	46.99519	prm !M_flo =AW("Ca")+2*AW("F");:78.0748064
4	FP	☑	55.74805	MVW(=M_flo S_flo / mol_f2_flo;, 1.000, 32.037`_0.105)
5	FP	☑	58.46684	
6	FP	☑	68.64915	
7	FP	☑	75.82188	
8	FP	☑	78.17045	
9	FP	☑	87.35751	
10	FP	☑	94.1873	

Figure 5
Equation (19) of the MSP method implemented in *TOPAS* (*a*) Launch Mode and *b*) GUI Mode, to quantify a phase of unknown lattice parameters.

Table 3
Example of quantifying any component phase according to the chemical composition of the whole mixture sample, using the MSP method.

	Mixture of cpd-1h		Corundum	Fluorite	Zincite
Chemical formula	$(Al_{0.693}Ca_{0.439}Zn_{0.369}O_{1.409}F_{0.878})_n$		Al_2O_3	CaF_2	ZnO
Molecular weight M_k	M_k/mol_f2 = 0.083		101.9613	78.0748	81.4084
MSP mol_f2			825.609	832.917	1443.86
Sum of LP-corrected intensity S_k	2004.9	= sum of	522.199	586.681	896.02
M_kS_k/mol_f2	166.4067	$\simeq$ sum of	64.4907	54.9935	50.5198
		wt%	37.93%	32.35%	29.72%

known to be due to the micro-absorption effect, in which the high-mass-absorption phase tends to be underestimated, while the low-mass-absorption phase tends to be overestimated.

4.4. Applying the MSP method for a phase of no known lattice parameter or chemical composition

Toraya (2017) pointed out [equation (20) therein] that it is still possible to quantify a phase of unknown crystal structure and unknown chemical composition if all the other phases have known scattering power per unit weight a_k^{-1}. This was based on the idea of treating the whole mixture as a single phase and deriving its chemical composition from either (1) the starting raw materials before reactions, (2) other elemental analysis techniques, *e.g.* X-ray fluorescence spectroscopy (XRF) *etc.*, or (3) scenarios elaborated in Section 3 of Toraya (2017).

Since equation (20) of the present paper has shown that the term M_k/mol_f2$_k$ in the current MSP method is essentially the same as a_k/C_k in DDM, a similar approach can be proposed and tested (see Table 3). The chemical composition of sample ‘cpd-1h’ based on the publicly available XRF data (see the *Data availability* section) is shown in the first row (left) of Table 3. Using the *TOPAS* INP template of supporting information Section S1, it is easy to calculate its ratio of M_k/mol_f2. With the sum of LP-corrected total intensity S_k of the ‘cpd-1h’ pattern, the value of M_kS_k/mol_f2 for the whole mixture sample can be calculated (second last row of Table 3), which is close to the sum of the same parameter calculated for the three individual phases on the right side of Table 3. Therefore, if any individual phase has unknown chemical composition (unknown M_k or mol_f2), it is still possible to derive its M_kS_k/mol_f2 value by subtracting the M_kS_k/mol_f2 value of other known phases from the total M_kS_k/mol_f2 value of the whole mixture sample. The weight percentages are just normalized M_kS_k/mol_f2 values.

4.5. Disordered kaolinite

Kaolinite KGa-2 is a poorly crystalline kaolinite source clay with stacking disorder (Sakharov *et al.*, 2016). The diffraction pattern of the mixture of this standard and 20 wt% corundum after homogenizing in a McCrone micronizer was measured using a Bruker D8 Advance diffractometer under Co $K\alpha$ radiation (40 kV, 40 mA). Dynamic Beam Optimization optics, including a variable divergence slit illuminating a 10 mm sample length and an automatic air-scattering knife above the sample, were used to eliminate air-scattering background and sample holder background, which helps in direct extraction of the scattering intensity of poorly crystalline phases. Soller slits (2.5°) were used on both primary and secondary sides of the beam path. A LynxEye XE-T detector (1D mode) was used to collect the diffraction signal from the sample spun at 15 rpm around the sample surface normal axis (to improve statistics) from 2 to 90° 2θ at a 0.015° step size in 1 h.

Fig. 6 compares the whole-pattern fits from Rietveld QPA using the kaolinite `str` model, from the C_k-corrected DDM calculation and from the MSP method (`hkl_Is`), for the above-described synthesized mixture of kaolinite KGa-2 source clay spiked with 20 wt% corundum. The QPA results obtained from each method are shown in the top right corners. Fig. 6(*a*) shows Rietveld QPA using the `str` structure model (Lee & Xu, 2020) with various peak profile corrections, including spherical harmonics correction for preferred orientation (Järvinen, 1993; Bruker, 2024), stacking fault modelling[2] (Ufer *et al.*, 2004; Wang *et al.*, 2012; Bruker, 2014; Coelho *et al.*, 2016; Bruker, 2017), and crystallite size broadening and microstrain broadening in *TOPAS* Launch Mode (INP file available in the supporting information). Figs. 6(*b*) and 6(*c*) show similar fits using the same `hkl_Is` model in GUI Mode, which generate the same S_k value (sum of LP-factor-corrected intensities). Stephens’ anisotropic peak broadening model (Stephens, 1999) for triclinic space groups was used in the ‘Microstructure’ tab of GUI Mode to fit the kaolinite asymmetric non-basal reflections. The difference between Figs. 6(*b*) and 6(*c*) is only in their QPA equations as described below, hence the slightly different phase weight percentages reported in their top-right corners. The *TOPAS* PRO files implemented with the C_k-corrected DDM and the MSP method (`hkl_Is`) are also available in the supporting information.

Since *TOPAS* v7, a ‘GUI Text’ tab has been added to its GUI, allowing users to implement custom equations within the *TOPAS* GUI Mode. The implementations of the C_k-corrected DDM method [equation (10)] and the MSP method [equation

---

[2] The *TOPAS* `Stack` macro containing the `stack` keyword was used to randomly shift the layer atoms flagged by the `layer` keyword in Cartesian **x**, **y**, **z** directions (stacking vector) in a supercell of 20 times the length of the *c* axis. The generated stacking layers have occupancies set to 0. The model is essentially a single-layer model in a supercell. However, the generated stacking layer atoms have geometric constraints set to avoid bumping into each other or into non-layer atoms, therefore keeping the model geometrically reasonable. With the keyword of `continue_after_convergence`, multiple refinements were executed before the result with the lowest $R_{\rm wp}$ was saved for the user.

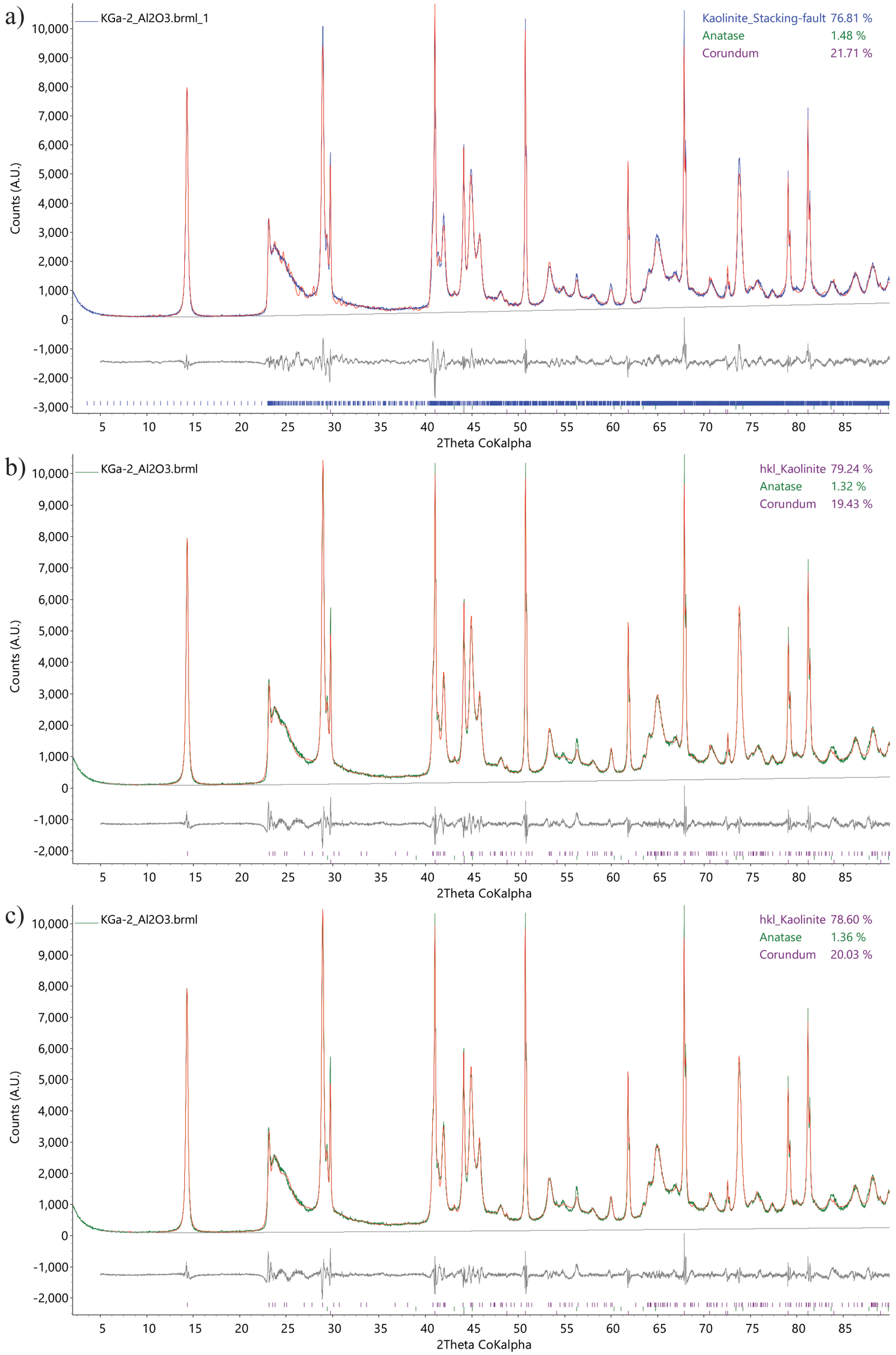

Figure 6
(*a*) Using the `str` structure model for kaolinite together with spherical harmonics for preferred orientation corrections, stacking fault modelling, crystallite size broadening and micro-strain broadening. $R_{\rm wp}$ 8.03%, goodness of fit (GOF) 2.67. (*b*) Using `hkl_Is` Pawley fitting and the proposed C_k-corrected DDM calculation [Fig. 7(*b*)] to quantify the kaolinite KGa-2 in synthetic mixture. $R_{\rm wp}$ 6.63%, GOF 2.19. (*c*) Same fitting except MSP QPA equations [Fig. 8(*a*)] are used. All fits used first-order Chebyshev background.

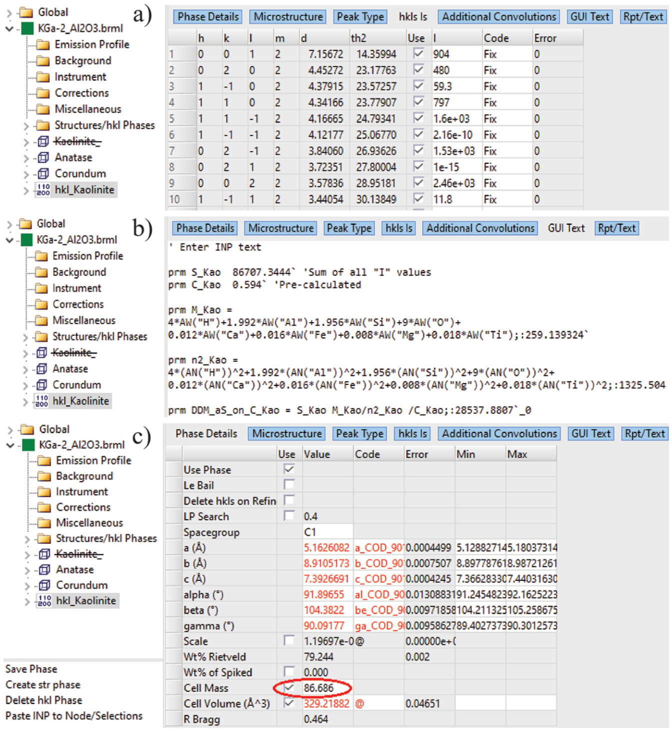

a)

	h	k	l	m	d	th2	Use	I	Code	Error
1	0	0	1	2	7.15672	14.35994	☑	904	Fix	0
2	0	2	0	2	4.45272	23.17763	☑	480	Fix	0
3	1	-1	0	2	4.37915	23.57257	☑	59.3	Fix	0
4	1	1	0	2	4.34166	23.77907	☑	797	Fix	0
5	1	1	-1	2	4.16665	24.79341	☑	1.6e+03	Fix	0
6	1	-1	-1	2	4.12177	25.06770	☑	2.16e-10	Fix	0
7	0	2	-1	2	3.84060	26.93626	☑	1.53e+03	Fix	0
8	0	2	1	2	3.72351	27.80004	☑	1e-15	Fix	0
9	0	0	2	2	3.57836	28.95181	☑	2.46e+03	Fix	0
10	1	-1	1	2	3.44054	30.13849	☑	11.8	Fix	0

b)

```
' Enter INP text

prm S_Kao  86707.3444` 'Sum of all "I" values
prm C_Kao  0.594` 'Pre-calculated

prm M_Kao =
4*AW("H")+1.992*AW("Al")+1.956*AW("Si")+9*AW("O")+
0.012*AW("Ca")+0.016*AW("Fe")+0.008*AW("Mg")+0.018*AW("Ti");:259.139324`

prm n2_Kao =
4*(AN("H"))^2+1.992*(AN("Al"))^2+1.956*(AN("Si"))^2+9*(AN("O"))^2+
0.012*(AN("Ca"))^2+0.016*(AN("Fe"))^2+0.008*(AN("Mg"))^2+0.018*(AN("Ti"))^2;:1325.504

prm DDM_aS_on_C_Kao = S_Kao M_Kao/n2_Kao /C_Kao;:28537.8807`_0
```

c)

	Use	Value	Code	Error	Min	Max
Use Phase	☑					
Le Bail	☐					
Delete hkls on Refin	☐					
LP Search	☐	0.4				
Spacegroup		C1				
a (Å)		5.1626082	a_COD_90	0.0004499	5.12882714	5.18037314
b (Å)		8.9105173	b_COD_90	0.0007507	8.89778761	8.98721261
c (Å)		7.3926691	c_COD_90	0.0004245	7.36628330	7.44031630
alpha (°)		91.89655	al_COD_90	0.01308831	91.2454823	92.1625223
beta (°)		104.3822	be_COD_9	0.00971858	104.211325	105.258675
gamma (°)		90.09177	ga_COD_9	0.00958627	89.4027373	90.3012573
Scale	☐	1.19697e-0	@	0.00000e+		
Wt% Rietveld		79.244		0.002		
Wt% of Spiked	☐	0.000				
Cell Mass	☑	86.686				
Cell Volume (Å^3)	☑	329.21882	@	0.04651		
R Bragg		0.464				

Figure 7
C_k-corrected DDM calculation in *TOPAS* GUI Mode: step (*a*) sum all `I` values from Pawley or Le Bail fitting using an `hkl_Is` phase; step (*b*) assign the sum to the parameter `S_Kao`; derive the `DDM_aS_on_C` value from the pre-calculated correction factor `C_Kao`, the molecule weight `M_Kao` and the sum of electron number squared for all atoms in the molecule `n2_Kao`; step (*c*) type in the value of `DDM_aS_on_C/Cell Volume` into the 'Cell Mass' box for this `hkl_Is` phase. Run the refinement again to obtain QPA results for all phases in this mixture.

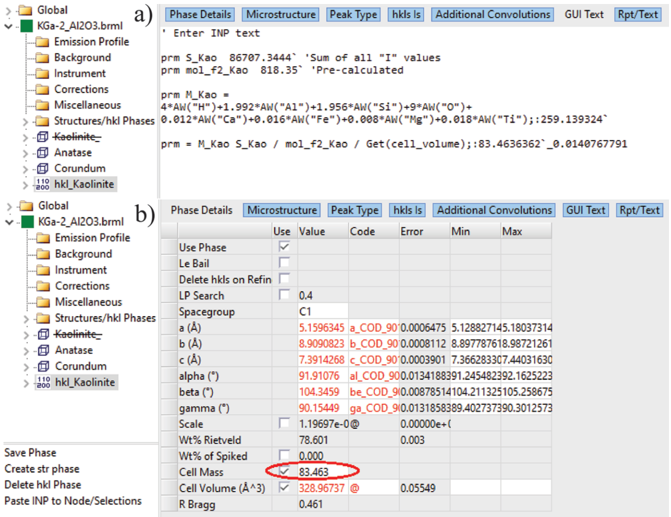

a)

```
' Enter INP text

prm S_Kao  86707.3444` 'Sum of all "I" values
prm mol_f2_Kao  818.35` 'Pre-calculated

prm M_Kao =
4*AW("H")+1.992*AW("Al")+1.956*AW("Si")+9*AW("O")+
0.012*AW("Ca")+0.016*AW("Fe")+0.008*AW("Mg")+0.018*AW("Ti");:259.139324`

prm = M_Kao S_Kao / mol_f2_Kao / Get(cell_volume);:83.4636362`_0.0140767791
```

b)

	Use	Value	Code	Error	Min	Max
Use Phase	☑					
Le Bail	☐					
Delete hkls on Refin	☐					
LP Search	☐	0.4				
Spacegroup		C1				
a (Å)		5.1596345	a_COD_90	0.0006475	5.12882714	5.18037314
b (Å)		8.9090823	b_COD_90	0.0008112	8.89778761	8.98721261
c (Å)		7.3914268	c_COD_90	0.0003901	7.36628330	7.44031630
alpha (°)		91.91076	al_COD_90	0.01341883	91.2454823	92.1625223
beta (°)		104.3459	be_COD_9	0.00878514	104.211325	105.258675
gamma (°)		90.15449	ga_COD_9	0.01318583	89.4027373	90.3012573
Scale	☐	1.19697e-0	@	0.00000e+		
Wt% Rietveld		78.601		0.003		
Wt% of Spiked	☐	0.000				
Cell Mass	☑	83.463				
Cell Volume (Å^3)	☑	328.96737	@	0.05549		
R Bragg		0.461				

Figure 8
MSP method in *TOPAS* GUI Mode: (*a*) assign the sum of `I` from `hkl_Is` fitting to the parameter `S_Kao`; calculate the `M_Kao S_Kao / mol_f2_Kao / Get(cell_volume)` value from the molecule weight `M_Kao` and the pre-calculated molecular scattering power `mol_f2_Kao`; (*b*) input the above-calculated value of `M_Kao S_Kao / mol_f2_Kao / Get(cell_volume)` into the 'Cell Mass' box for this `hkl_Is` phase. Run the refinement again to obtain QPA results for all phases in this mixture.

(19)] in the *TOPAS* GUI Mode for this example are shown in Figs. 7(*b*) and 8(*a*), respectively.

To minimize peak-area correlation with the background, only the first-order Chebyshev polynomials were refined for background across all methods. Both new approaches yielded comparable QPA results to those from the conventional Rietveld QPA, which is significantly more complex in disordered structural modelling and corrections. Note that the MSP method was design for analysing full-range XRD patterns (Li *et al.*, 2022; Li & He, 2023). Applying the method to a relatively narrow 2θ range (2–90°) in this example may reduce its accuracy. Nevertheless, the discrepancies between the quantified corundum weight percentages and its known values are lower than 2 wt%.

In the example shown in Fig. 8, the unit-cell volume is effectively cancelled out when the *TOPAS* QPA routine calculates the product of cell mass and cell volume. As a result, it is not explicitly required in the MSP QPA equation, *i.e.* equation (19). In this case, the unit-cell parameter is used solely to achieve a good fit to the kaolinite KGa-2 pattern, ensuring accurate S_k extraction. The next example will demonstrate the scenario in which the lattice parameters of the unknown crystal structure phase are not used through the MSP method (`xo_Is`).

4.6. Disordered chlorite

The aforementioned corrections applied to the crystal structure in conventional Rietveld QPA may not adequately account for other complex structural disorders. An illustrative example is the clay mineral ripidolite, which represents an intermediate chlorite group member between chamosite (Fe-rich) and clinochlore (Mg-rich). Chlorite CCa-2 is a crystalline ripidolite source clay with cationic disorder (Gailhanou *et al.*, 2009). The chemical formula of CCa-2 derived from the chemical composition reported therein is $Ca_{0.022}(Fe_{3.682}Mg_{5.650}Mn_{0.022}K_{0.013}Na_{0.039}Ti_{0.117}P_{0.003})(Si_{5.040}Al_{4.753})O_{20}(OH)_{16}$, with a molecular weight of 1214.033 g mol^{-1}. The MSP of this formula is calculated as 4303.128, using the *TOPAS* file `cal_mol_f2_CCa-2_Co.inp` (available in the supporting information).

The diffraction pattern of the mixture of this standard and 20 wt% corundum after homogenizing in a McCrone micronizer was measured using a Bruker D8 Endeavor ECO diffractometer under Co *Kα* radiation (35 kV, 28 mA). Dynamic Beam Optimization optics, including a variable divergence slit at 15 mm sample illumination length and an automatic air-scattering knife above the sample, were used to eliminate air-scattering background and sample holder background, which helps in direct extraction of the scattering intensity of poorly crystalline phases. Soller slits (4.1°) were used on both primary and secondary sides of the beam path. A LynxEye XE-T detector (1D mode) was used to collect the diffraction signal from the sample spun at 15 rpm around the sample surface normal axis (to improve statistics) from 2 to 90° 2θ at a 0.015° step size in 1 h.

Fig. 9 compares the whole-pattern fitting from Rietveld QPA using the clinochlore `str` model (Zanazzi *et al.*, 2007)

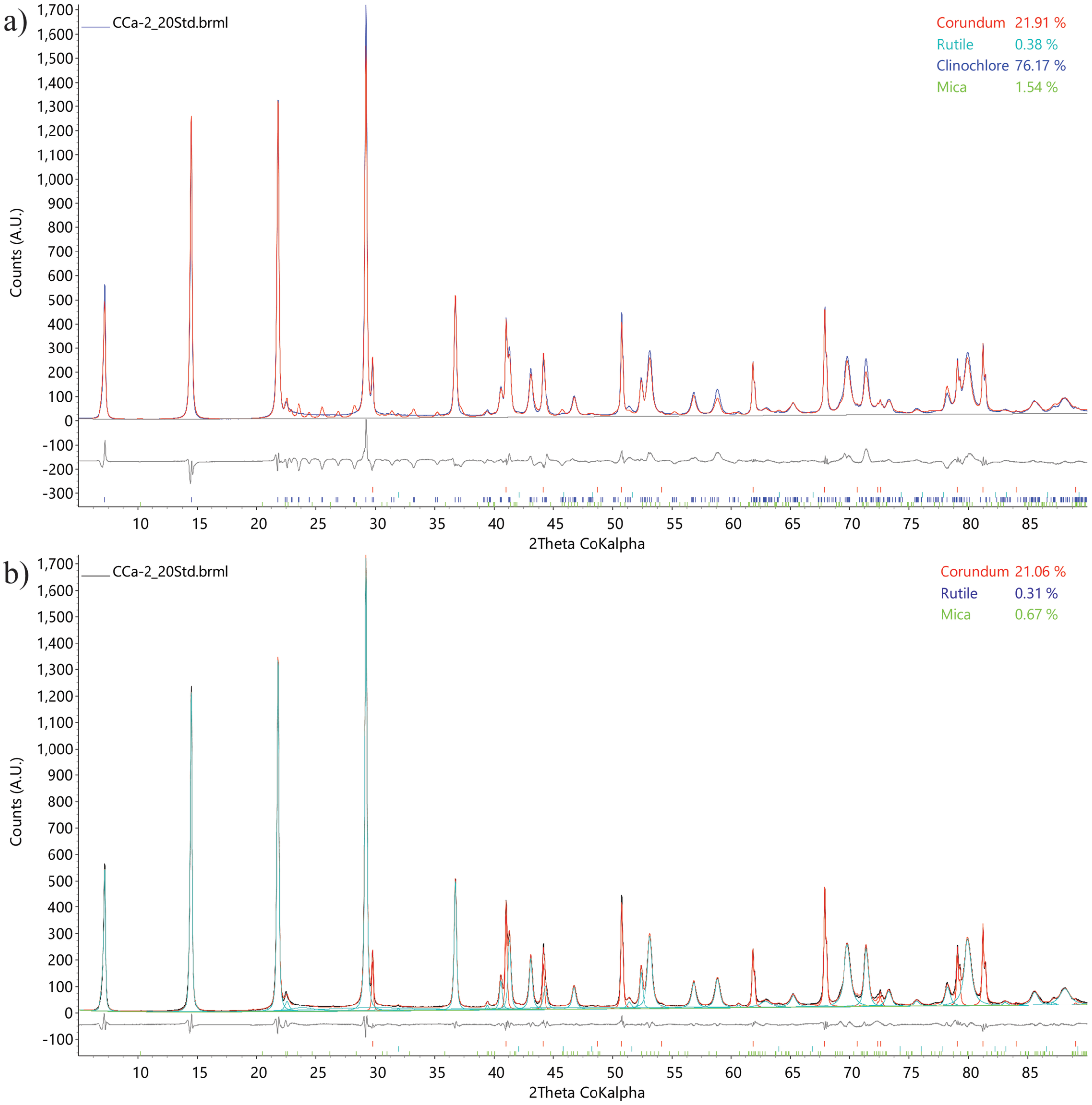

Figure 9
(*a*) Using the `str` structure model for ripidolite CCa-2 together with Stephens' anisotropic peak broadening model. $R_{\rm wp}$ 13.76%, GOF 12.21; (*b*) Using `xo_Is` peak fitting for the MSP method (Fig. 10). $R_{\rm wp}$ 5.45%, GOF 4.87. All fits used a first-order Chebyshev background.

and from the MSP method (`xo_Is`) for the above-described synthesized mixture of ripidolite CCa-2 source clay spiked with 20 wt% corundum. As can be seen from Fig. 9(*a*), many non-basal reflections calculated from the clinochlore `str` crystal structure that ought to be present between 20 and 30° 2θ are completely missing in the measured data. Stephens' anisotropic peak broadening correction is applied but still not able to handle such a large discrepancy. In contrast, a much superior fit is achieved in Fig. 9(*b*) using the MSP method (`xo_Is`), because it allows more flexible individual peak profiles to be refined.

The QPA results in the top-right corner of Fig. 9(*a*) overestimate corundum. In contrast, Fig. 9(*b*) shows slightly more accurate QPA results for corundum obtained through the model-free MSP (`xo_Is`) approach. The calculated weight percent of ripidolite CCa-2 [78.0 (2) wt%] is shown in the `MVW` macro in Fig. 10.

In Fig. 10, the sum of `I` values extracted using the `xo_Is` model `pks_CCa-2` is assigned to S_k using the `prm_with_error` keyword to take into account the errors from the intensity extraction. With the molecular scattering power mol_f2$_k$ calculated above and the formula weight M_k calculated using `AW` macros, M_kS_k/mol_f2$_k$ [equation (19)] can be used as the `cell_mass` in the `MVW` macro, as described in Section 3.2 step (*c*).

The `CCa-2_20Std.pro` file used for this calculation is provided in the supporting information.[3] In this example, the proposed MSP method employs the peaks phase `xo_Is` model to extract the diffraction intensities of CCa-2 and calculate its molecular scattering power only from its

---

[3] For the purpose of reloading, *TOPAS* replaces the quotation marks with '§', and replaces the divide mark '/' with '£' in the `.pro` file. Users need to replace them back once the `.pro` file has been loaded into *TOPAS*.

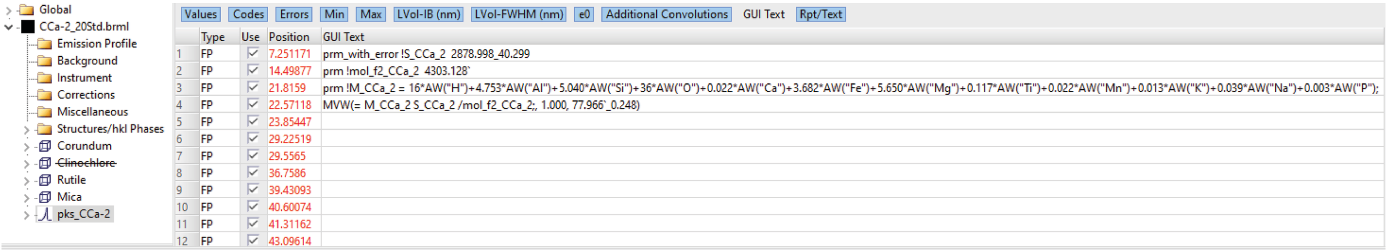

	Type	Use	Position	GUI Text
1	FP	☑	7.251171	prm_with_error !S_CCa_2 2878.998_40.299
2	FP	☑	14.49877	prm !mol_f2_CCa_2 4303.128`
3	FP	☑	21.8159	prm !M_CCa_2 = 16*AW("H")+4.753*AW("Al")+5.040*AW("Si")+36*AW("O")+0.022*AW("Ca")+3.682*AW("Fe")+5.650*AW("Mg")+0.117*AW("Ti")+0.022*AW("Mn")+0.013*AW("K")+0.039*AW("Na")+0.003*AW("P");
4	FP	☑	22.57118	MVW(= M_CCa_2 S_CCa_2 /mol_f2_CCa_2;, 1.000, 77.966`_0.248)
5	FP	☑	23.85447	
6	FP	☑	29.22519	
7	FP	☑	29.5565	
8	FP	☑	36.7586	
9	FP	☑	39.43093	
10	FP	☑	40.60074	
11	FP	☑	41.31162	
12	FP	☑	43.09614	

Figure 10
In the last macro, `MVW`, the first parameter is 'Cell mass', written as M_kS_k/mol_f2$_k$; the 2nd parameter `1.000` represents the unit-cell volume of the `xo_Is` model; the third parameter shows the refined QPA result for ripidolite CCa-2: 78.0 (2) wt%.

published chemical composition. No information on lattice parameters or atomic positions was used. The MSP method is both simpler and more accurate than conventional Rietveld QPA for quantifying the poorly crystalline clay mineral CCa-2 ripidolite.

5. Discussion

In the diffraction pattern of a multi-phase mixture, peak overlaps are inevitable. By using crystal structural models for known crystalline phases, we can subtract their intensities from the overlapping peaks, allowing the remaining intensity to be allocated to a Pawley or Le Bail fit for a poorly crystalline or disordered phase. This combined refinement was also adopted by Toraya (2018, 2019), who used peaks phase `xo_Is` and Pawley phase `hkl_Is` (Type A fitting function therein) and Rietveld modelling or intensity data from databases (Type B fitting function therein) alongside pre-measured scans using the *FULLPAT* method (Chipera & Bish, 2002) (Type C fitting function therein), all integrated within a single refinement. This approach is considered superior to applying Type A fitting functions to all phases, where the partitioning of overlapping peak intensities among contributing phases heavily depends on the partitioning strategy. The iterative 'volume-proportional partitioning' strategy (Toraya, 2016) still requires an initial assumption of equal partitioning, which may face problems when the primary diffraction peaks of an unknown phase significantly overlap with those of other phases.

In conventional Rietveld QPA, the structure factor of each *hkl* reflection can be calculated from the known crystal structures of the constituent phases, allowing for the reconstruction of XRD patterns (Hill & Howard, 1987). In addition to determining the weight percentages of component phases (QPA), Rietveld QPA also provides valuable information on crystallite size, microstrain, preferred orientation, atomic displacement parameters, atomic occupancies and atomic positions, among other structural characteristics. In this context, knowledge of the crystal structure serves as a sufficient but not a necessary condition for QPA. QPA can still be performed as long as the total structure factors, or the scattering power per unit mass of the analyte, can be either calculated or experimentally calibrated.

The application field of the currently proposed C_k-corrected DDM is limited to poorly crystalline phases, as it still relies on the crystal structure being close enough to disorder free to calculate the C_k values. In contrast, the MSP method totally eliminates the need for information on atomic positions, lattice parameters, unit-cell volume or the number of molecules per unit cell. Instead, it requires only the chemical composition of the unknown phase.

Both of the proposed methods are classified as 'direct' QPA methods (Madsen *et al.*, 2011), which require accurate separation of pattern background from phase contributions. In the present examples, the proposed methods are shown to be effective for analysing XRD powder patterns collected using a variable divergence slit. The use of Dynamic Beam Optimization optics suppresses non-sample scattering background, thereby facilitating the direct extraction of the scattering intensity of poorly crystalline phases. Additionally, a very low order Chebyshev polynomial (only first order) was used to model the pattern background, further reducing the correlation of background with intensity S_k extracted via Pawley fitting or peaks phase fitting. In the case of applying a 'direct' QPA method to an amorphous phase, the separation of phase contributions from background becomes more challenging and typically necessitates experimental calibration. In such cases, the PONKCS method and the internal standard method remain more efficient alternatives. Effective background determination methods for multi-phase mixtures have been reported (Madsen *et al.*, 2011; Toraya, 2019; Toraya & Omote, 2019) and can be adopted.

The proposed C_k-corrected DDM and MSP methods both omit the electron density in interatomic bonds, which may explain their discrepancy with the Rietveld method. Rietveld QPA is still considered to be the most accurate QPA method, supported by Table 2, in which methods with more 'R' yield more accurate QPA results. However, if the accuracies of QPA results obtained from the two currently proposed C_k-corrected DDM and MSP methods (absolute deviation within ±3 wt%) are deemed acceptable, they could be widely applied to quantify poorly crystalline, disordered phases or partially or no known crystal structures. Such cases would otherwise require complex explicit structural modelling or corrections, or laborious experiment calibration. The two proposed methods thus hold significant potential for, especially, industrial applications.

6. Conclusion

Analysing the equations of the direct derivative method (Toraya, 2016) reveals that the a_kS_k/C_k term in DDM terminology is essentially equivalent to the $Z_kM_kV_k$ Scale_k factor in the conventional Rietveld QPA method. Incorporating individual C_k factors for different phases enhances the accuracy of the original DDM calculations, particularly for mixtures with high atomic-number contrast. Similarly, analysing the equations of the original unit-cell scattering power method (Li *et al.*, 2022) enables its simplification into a molecular scattering power method, where $M_kS_k/\mathrm{mol\_f2}_k$ is equivalent to the $Z_kM_kV_k\mathrm{Scale}_k$ factor in conventional Rietveld QPA. The MSP method eliminates the need for knowledge of the number of molecules per unit cell, lattice parameters and unit-cell volume. While the MSP method endorses the concept of C_k-corrected DDM, the MSP method does not require C_k calculations to relate to the squared electron numbers of atoms in the molecule. Instead, the MSP method determines molecular scattering power by summing the atomic scattering powers (the sum of squared product of atomic form factor and atomic displacement parameter).

APPENDIX *A*

Meanings and relationships of the reserved intensity parameters in *TOPAS*

The *TOPAS* v7 software defines various reserved parameters concerning diffraction intensity for *hkl* reflections, including `numerical_area`, `I_no_scale_pks`, `Iobs_no_scale_pks`, `I_after_scale_pks`, `I` *etc*. Their meanings are summarized as below and are illustrated through a refinement of the `corundum.raw` data publicly available from the IUCr CPD QPA round robin (https://www.iucr.org/__data/iucr/powder/QARR/intro.htm).

(1) `numerical_area` returns a value of direct integration (counts × degrees) for the observed diffraction peak or diffraction pattern over the fitted 2θ range. This is similar to the 'net area' (cps × degrees) parameter in the *DIFFRAC.EVA* software calculated from the measured XRD pattern.

(2) `I_no_scale_pks` equals the product of 'scale factor', 'multiplicity' and squared structure factor $|F|^2$ for each *hkl* reflection in the `str` structure model. This parameter does not contain the LP factor and therefore reflects the nature of the phase itself.

(3) `Iobs_no_scale_pks` partitions the measured intensity $Y_{\rm obs}$ at each 2θ step into the contributing phases, according to the ratio of their intensity contribution at that 2θ step. This parameter has the LP factor removed from the measured intensities. Therefore, when a good fit is achieved, this value should be close to the `I_no_scale_pks` value. This parameter is equivalent to the `I` parameter in `hkl_Is`, `xo_Is` and `d_Is` phases.

(4) `I_after_scale_pks` is equal to the product of `I_no_scale_pks` and all the `scale_pks` terms, including the LP factor. When a good fit is achieved, the value of `I_after_scale_pks` should be close to the `numerical_area` value for the same fitted 2θ range.

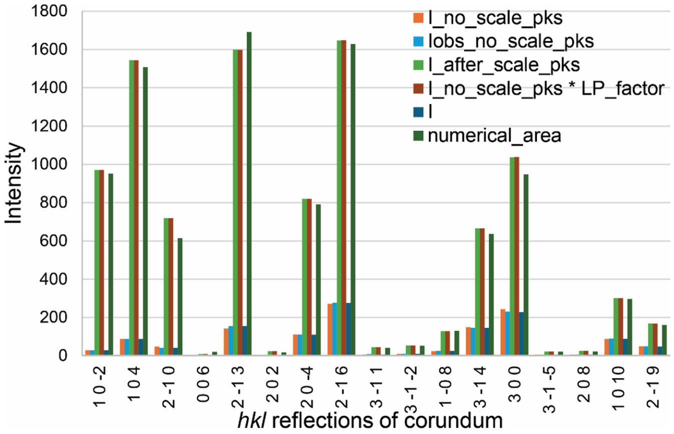

Figure 11
Comparison of the reserved intensity parameters in *TOPAS* from a refinement of the powder diffraction pattern `corundum.raw` in the IUCr CPD round robin. The five histograms for each *hkl* reflection follow the order of the legend.

The `I` and `numerical_area` for each corundum diffraction peak extracted using the *TOPAS* file `extract_numerical_area.inp` (available in the supporting information) and the other three intensity parameters `I_no_scale_pks`, `Iobs_no_scale_pks` and `I_after_scale_pks` extracted using the *TOPAS* file `extract_Is.inp` (available in the supporting information) are compared in Fig. 11. It is obvious that the LP factor defined in `TOPAS.inc` forms the ratio between any group 1 parameter (`numerical_area`, `I_after_scale_pks`) and any group 2 parameter (`I_no_scale_pks`, `Iobs_no_scale_pks`, `I`) in `hkl_Is`/`xo_Is` phases.

$$\text{LP factor} = \frac{1+\cos^2\theta_{\rm m}\cos^2 2\theta}{\sin^2\theta\cos\theta},$$

where $\theta_{\rm m}$ represent the 2θ angle for the monochromator; θ is the Bragg angle of the *hkl* reflection.

Therefore, it is clear that the `numerical_area` value in *TOPAS* is not equivalent to the value $S_k = \sum_j I_{jk}\, G_{jk}$ in DDM, because `numerical_area` does not have the LP factor, which is defined as G_{jk}^{-1} by Toraya (2016), removed. DDM macros based on the `numerical_area` parameter are not equivalent to implementations of the direct derivation method (Toraya, 2016). The sum of `I` values in the *TOPAS* `xo_Is` or `hkl_Is` models should be used to calculate the S_k value in DDM.

Acknowledgements

The first author expresses sincere gratitude to his QPA mentor, Mr Ian C. Madsen, for an inspiring conversation and valuable personal communications regarding the concept of the dummy cell. The first author also appreciates the constructive discussions with Dr Matthew Rowles at the IUCr 2023 Congress and during the funeral of our esteemed tutor, the late Emeritus Professor Brian O'Connor of Curtin University. The experimental data presented in this study were collected with the support from the Central Analytical Research Facility (CARF) at Queensland University of Technology (QUT). The time and efforts of two anonymous reviewers in reviewing the manuscript were appreciated. Open access publishing facilitated by Queensland University of Technology, as part of the Wiley–Queensland University of Technology agreement via the Council of Australian University Librarians.

Conflict of interest

The authors declare there are no conflicts of interest.

Data availability

IUCr CPD round robin data are available at https://www.iucr.org/__data/iucr/powder/QARR/intro.htm. All other data and models supporting the results reported in this article are published in the supporting material.

References

Bish, D. L. & Howard, S. A. (1988). *J. Appl. Cryst.* **21**, 86–91.

Bruker (2014). *DIFFRAC.TOPAS 5 technical reference 9.10*, *Stacking faults*, p. 103. Bruker AXS GmbH, Karlsruhe, Germany.

Bruker (2017). *DIFFRAC.TOPAS 6 technical reference 9.10*, *Stacking faults*, p. 123. Bruker AXS GmbH, Karlsruhe, Germany.

Bruker (2024). *DIFFRAC.TOPAS 7 technical reference 13.6.3*, *Spherical harmonics*, p. 284. Bruker AXS GmbH, Karlsruhe, Germany.

Chipera, S. J. & Bish, D. L. (2002). *J. Appl. Cryst.* **35**, 744–749.

Coelho, A. A. (2018). *J. Appl. Cryst.* **51**, 210–218.

Coelho, A. A., Evans, J. S. O. & Lewis, J. W. (2016). *J. Appl. Cryst.* **49**, 1740–1749.

Gailhanou, H., Rogez, J., Miltenburg, J. C., Genderen, A. C. G., Grenèche, J. M., Gilles, C., Jalabert, D., Michau, N., Gaucher, E. C. & Blanc, P. (2009). *Geochim. Cosmochim. Acta* **73**, 4738–4749.

He, M. & Li, H. (2022). *J. Appl. Cryst.* **55**, 436–438.

Hettich, A. (1935). *Z. Kristallogr. Cryst. Mater.* **91**, 154–156.

Hill, R. J. & Howard, C. J. (1987). *J. Appl. Cryst.* **20**, 467–474.

Hughes, H. K. (1965). *Am. J. Phys.* **33**, 99–101.

Järvinen, M. (1993). *J. Appl. Cryst.* **26**, 525–531.

Kartha, G. (1953). *Acta Cryst.* **6**, 817–820.

Lee, S. & Xu, H. (2020). *Minerals* **10**, 124.

Li, H. & He, M. (2023). *J. Appl. Cryst.* **56**, 1707–1713.

Li, H., He, M. & Zhang, Z. (2022). *Powder Diffr.* **37**, 34–39.

Madsen, I. C. & Scarlett, N. V. Y. (2008). *Powder diffraction: theory and practice*, edited by R. E. Dinnebier & S. J. L. Billinge, ch. 11, pp. 298–331. The Royal Society of Chemistry.

Madsen, I. C., Scarlett, N. V. Y., Cranswick, L. M. D. & Lwin, T. (2001). *J. Appl. Cryst.* **34**, 409–426.

Madsen, I. C., Scarlett, N. V. Y. & Kern, A. (2011). *Z. Kristallogr.* **226**, 944–955.

Pollard, S. (1926). *Proc. London Math. Soc.* **s2–25**, 237–246.

Sakharov, B. A., Drits, V. A., McCarty, D. K. & Walker, G. M. (2016). *Clays Clay Miner.* **64**, 314–333.

Sayre, D. (1951). *Acta Cryst.* **4**, 362–367.

Scarlett, N. V. Y. & Madsen, I. C. (2006). *Powder Diffr.* **21**, 278–284.

Stephens, P. W. (1999). *J. Appl. Cryst.* **32**, 281–289.

Toraya, H. (2016). *J. Appl. Cryst.* **49**, 1508–1516.

Toraya, H. (2017). *J. Appl. Cryst.* **50**, 820–829.

Toraya, H. (2018). *J. Appl. Cryst.* **51**, 446–455.

Toraya, H. (2019). *J. Appl. Cryst.* **52**, 520–531.

Toraya, H. (2021). *Powder Diffr.* **36**, 159–168.

Toraya, H. (2022). *J. Appl. Cryst.* **55**, 439–441.

Toraya, H. & Omote, K. (2019). *J. Appl. Cryst.* **52**, 13–22.

Ufer, K., Roth, G., Kleeberg, R., Stanjek, H., Dohrmann, R. & Bergmann, J. (2004). *Z. Kristallogr.* **219**, 519–527.

Wang, X., Hart, R. D., Li, J., McDonald, R. G. & van Riessen, A. (2012). *J. Appl. Cryst.* **45**, 1295–1302.

Wang, X., Li, J., Hart, R. D., van Riessen, A. & McDonald, R. (2011). *J. Appl. Cryst.* **44**, 902–910.

Zanazzi, P. F., Montagnoli, M., Nazzareni, S. & Comodi, P. (2007). *Am. Mineral.* **92**, 655–661.

Zwillinger, D. (2014). *Table of integrals, series and products*, 8th ed. Academic Press.